New constraints on radiative decay of long-lived particles in big bang nucleosynthesis with new ^{4}He photodisintegration data

Motohiko Kusakabe,[1,2,*,†] Toshitaka Kajino,[1,2,3] Takashi Yoshida,[1] Tatsushi Shima,[4] Yasuki Nagai,[4] and Toshiteru Kii[5]

[1]*Division of Theoretical Astronomy, National Astronomical Observatory of Japan, Mitaka, Tokyo 181-8588, Japan*
[2]*Department of Astronomy, Graduate School of Science, University of Tokyo, Hongo, Bunkyo-ku, Tokyo 113-0033, Japan*
[3]*Department of Astronomical Science, The Graduate University for Advanced Studies, Mitaka, Tokyo 181-8588, Japan*
[4]*Research Center for Nuclear Physics, Osaka University, Ibaraki, Osaka 567-0047, Japan*
[5]*Institute of Advanced Energy, Kyoto University, Gokasyo, Uji, Kyoto 611-0011, Japan*

(Received 24 June 2008; revised manuscript received 1 May 2009; published 19 June 2009)

A recent measurement of ^{4}He photodisintegration reactions, ^{4}He$(\gamma, p)^3$H and ^{4}He$(\gamma, n)^3$He with laser-Compton photons shows smaller cross sections than those estimated by other previous experiments at $E_\gamma \lesssim 30$ MeV. We study big bang nucleosynthesis with the radiative particle decay using the new photodisintegration cross sections of ^{4}He as well as previous data. The sensitivity of the yields of all light elements D, T, ^{3}He, ^{4}He, ^{6}Li, ^{7}Li, and ^{7}Be to the cross sections is investigated. The change of the cross sections has an influence on the nonthermal yields of D, ^{3}He, and ^{4}He. On the other hand, the nonthermal ^{6}Li production is not sensitive to the change of the cross sections at this low energy, since the nonthermal secondary synthesis of ^{6}Li needs energetic photons of $E_\gamma \gtrsim 50$ MeV. The nonthermal nucleosynthesis triggered by the radiative particle decay is one of candidates of the production mechanism of ^{6}Li observed in metal-poor halo stars. In the parameter region of the radiative particle lifetime and the emitted photon energy, which satisfies the ^{6}Li production above the abundance level observed in metal-poor halo stars, the change of the photodisintegration cross sections at $E_\gamma \lesssim 30$ MeV as measured in the recent experiment leads to $\sim$10% reduction of resulting ^{3}He abundance, whereas the ^{6}Li abundance does not change for this change of the cross sections of ^{4}He$(\gamma, p)^3$H and ^{4}He$(\gamma, n)^3$He. The ^{6}Li abundance, however, could show a sizable change and therefore the future precise measurement of the cross sections at high energy $E_\gamma \gtrsim$ 50 MeV is highly required.

DOI: 10.1103/PhysRevD.79.123513 PACS numbers: 25.10.+s, 26.35.+c, 98.80.Cq, 98.80.Es

I. INTRODUCTION

In standard cosmology, the Universe is thought to have experienced big bang nucleosynthesis (BBN) at a very early stage. The light nuclides D, T + ^{3}He, ^{4}He, and ^{7}Li + ^{7}Be are produced in the standard BBN (SBBN) at observable levels, while this model does not make appreciable quantities of ^{6}Li. The WMAP satellite has measured the temperature fluctuations of the cosmic microwave background (CMB) radiation, and parameters characterizing the standard big bang cosmology have been deduced [1,2] from these data. For the baryon-to-photon ratio $\eta_{\rm CMB}$ deduced from fits to the CMB, the BBN model predicts abundances of the light elements except for ^{6}Li and ^{7}Li, which are more-or-less consistent with those inferred from astronomical observations.

Spectroscopic lithium abundances have been detected in the atmospheres of metal-poor stars. Nearly constant abundances of ^{6}Li and ^{7}Li in metal-poor Population II (Pop II) stars have been inferred. There is about a factor of 3 under abundance of ^{7}Li in metal-poor halo stars (MPHSs) with respect to the SBBN prediction when using the baryon-to-photon ratio $\eta_{\rm CMB}$. This is called the ^{7}Li problem [3–5]. In addition, spectroscopic measurements obtained with high resolution indicate that MPHSs have a very large abundance of ^{6}Li, i.e., at a level of about 3 orders of magnitude larger than the SBBN prediction of the ^{6}Li abundance, which is called the ^{6}Li problem [5,6]. Cayrel *et al.* [7] studied line asymmetries to be generated by convective Doppler shifts in stellar atmospheres, and found that the convective asymmetry might mimic the presence of ^{6}Li, and an error of ^{6}Li/^{7}Li amounts to a few percent that is roughly comparable to the values estimated from MPHSs. The ^{6}Li problem, therefore, may not exist in fact, since the convective asymmetry could give a possible solution to the ^{6}Li problem within the framework of SBBN.

The possibility of ^{6}Li production in nonstandard BBN triggered by the decay of unstable relic neutral massive particles X has been studied [8–16]. Several critical constraints on the properties of X particles were derived from the studies of radiative decay [9–12], hadronic decay, or annihilation [13–16] of X particles along with the BBN constraints on the light elements. These particle decay induces electromagnetic and/or hadronic showers triggering the destruction of preexisting nuclei and the production of different nuclear species. A recent detailed study [12] of the radiative decay and its influence on the ^{6}Li production has found a parameter region of lifetime $\tau_X \sim 10^8$–10^{12} s

*Research Fellow of the Japan Society for the Promotion of Science
†kusakabe@th.nao.ac.jp

and abundance parameter $\zeta_X \sim 10^{-13}$–10^{-12} GeV where the nonthermal nucleosynthesis of ^{6}Li can explain the observed abundance level in MPHSs. This parameter region satisfies the two observational constraints on the CMB energy spectrum and the primordial light element abundances. Three important characteristics were found for the interesting parameter region. First, ^{3}He and t are the seeds for ^{6}Li in the processes ^{4}He(^{3}He, p)^{6}Li and ^{4}He(t, n)^{6}Li. Second, the excess of ^{6}Li abundance is therefore regulated by the amounts of ^{3}He and t that are produced by the nonthermal photodisintegration of ^{4}He, i.e., ^{4}He(γ, p)^{3}H and ^{4}He(γ, n)^{3}He. Hence, the radiative decay model that results in ^{6}Li production above the MPHS abundance level is also reflected by an enhancement of the ^{3}He abundance with respect to the SBBN value. Third, the radiative decay does not resolve the ^{7}Li problem [17]. It is therefore concluded that other mechanisms such as the stellar depletion of the lithium isotopes in the atmosphere of MPHSs [19,20] or new burst of late-time BBN on the exotic X-bound nuclei in the case of negatively charged leptonic particles X^- [21–35] must operate to lower the ^{7}Li abundance.

A recent measurement of ^{4}He photodisintegration reactions ^{4}He(γ, p)^{3}H and ^{4}He(γ, n)^{3}He with laser-Compton photons [36] shows much smaller cross sections than those estimated from the other previous experiments [37] and those summarized in Ref. [11] at the photon energies 20 MeV $\lesssim E_\gamma \lesssim$ 30 MeV. If these nonthermal photon energies dominate the destruction of ^{4}He, the production of ^{3}He and t and also the subsequent production of ^{6}Li via ^{4}He(^{3}He, p)^{6}Li and ^{4}He(t, n)^{6}Li, this would change the parameter region of τ_X and ζ_X of massive relic particles X so that the resultant nonthermal nucleosynthesis of ^{6}Li can explain the abundance level observed in MPHSs. The first purpose of this article is to study the sensitivity of nonthermal BBN of all light elements D, T, ^{3}He, ^{4}He, ^{6}Li, ^{7}Li, and ^{7}Be to the photodisintegration cross sections of ^{4}He. The second purpose is to infer the uncertainties of the two parameters τ_X and ζ_X of massive relic particles X, which would arise from the uncertainties of the measured reaction cross sections.

In Sec. II, we present a result of a new measurement of ^{4}He photodisintegration cross sections. In Sec. III, we briefly explain the model of nonthermal nucleosynthesis and the calculated result of the effect of the considered change of the photodisintegration cross sections. In Sec. IV, we summarize our conclusion and offer an outlook for measurements of ^{4}He photodisintegration.

II. ^{4}He(γ, p)^{3}H AND ^{4}He(γ, n)^{3}He CROSS SECTIONS

So far the cross section data of the photodisintegration of ^{4}He have been obtained from the direct photodisintegration experiments as well as the inverse radiative capture experiments. Indirect probes such as the (p, p') reaction [38] and the (^{7}Li, ^{7}Be) reaction [37] have also been applied to investigate the property of the dipole excitations of ^{4}He.

The direct experiments have been performed by detecting either charged fragments (p, ^{3}H, ^{3}He) or neutrons from the photodisintegration reactions. As incident real photon beams, either continuous bremsstrahlung photons or quasimonochromatic ones generated with various methods such as the photon tagging, the positron annihilation in flight, and the laser Compton backscattering were used. Since the energies of the emitted particles are small due to high threshold energies of the photodisintegrations of ^{4}He, many efforts have been devoted to detect those particles clearly from the backgrounds caused by the incident high-energy γ rays. In the inverse experiments, the reaction cross sections are much smaller than the photodisintegrations because of the difference of the phase space factors, and therefore the measurements have been performed with great care to the influence of the background γ rays as well as the determinations of the experimental parameters such as the detector efficiency for high-energy capture γ rays, the effective target thicknesses, the incident beam intensity, and so on.

In spite of the above experimental efforts, there have been large discrepancies in the previous data as shown in Fig. 1. Especially in the energy region below ~30 MeV, the data show either a pronounced peak at around 25–26 MeV or a rather smooth curve as a function of the excitation energy. In order to determine the cross sections more accurately, Shima *et al.* recently performed measurements using quasimonochromatic laser-Compton photons and a time projection chamber containing a gas mixture of He and CD_4 [36,39,40]. The method had the following features:

(i) Thanks to the quasimonochromatic and well-collimated γ-ray beam, the background due to low-energy γ rays is very small.
(ii) Since the time projection chamber gas serves as an active target, low-energy charged fragments from the photodisintegrations can be detected simultaneously for ^{4}He(γ, p) and ^{4}He(γ, n), with efficiencies of nearly 100% and a solid angle of 4π.
(iii) The absolute sensitivity of the measurement can be accurately checked with the D(γ, n)p reaction, whose cross section is well known in the energy region of the present interest.

Previously, Shima *et al.* measured the cross sections in the γ-ray energy region from 20 to 30 MeV using the laser-Compton γ-ray source at the National Institute of Advanced Industrial Science and Technology (AIST) [36].

As shown in Fig. 1, the cross sections from the experiments are found to monotonically increase as a function of the γ-ray energy up to ~30 MeV, being quite different from the standard fitting functions previously evaluated by Cyburt *et al.* [11]. With the above mentioned situation in mind, the sensitivity of the BBN to the photodisintegration

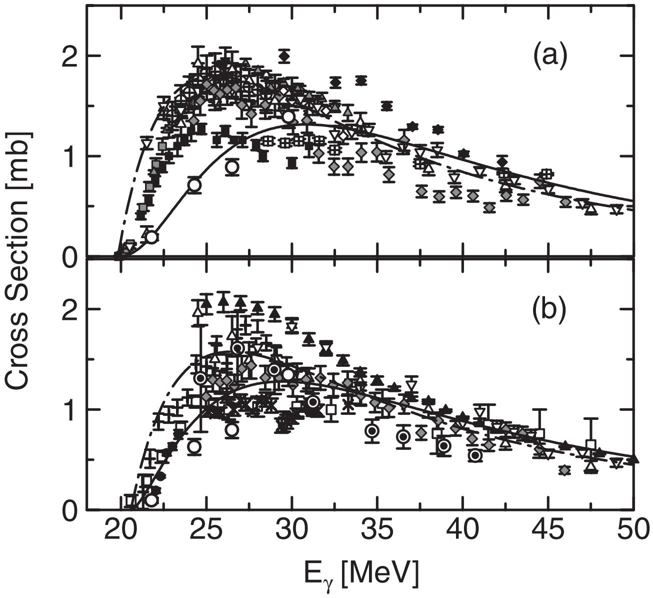

FIG. 1. The cross sections of the ^{4}He$(\gamma, p)^3$H (upper panel: a) and ^{4}He$(\gamma, n)^3$He (lower panel: b) reactions. The open circles stand for the published data [36] from experiments performed using quasimonochromatic laser-Compton photon beams at AIST. The dotted circles are the latest data of the (γ, n) reaction measured by means of a tagged photon beam [64]. The other symbols indicate the previous data (see the references in Ref. [36]). The error bars show 1σ uncertainties in the cross section data. The solid curves are the most probable excitation functions determined from the experimental data at $E_\gamma \lesssim$ 30 MeV [36] and the previous ones at higher energies 30 MeV $\lesssim E_\gamma \lesssim$ 116 MeV [41–43]. The dashed-dotted curves are the fitting functions to some of the available data summarized in Ref. [11].

cross sections of ^{4}He was studied in the present paper by using the recent experimental results as well as the previously adopted standard fitting functions in Ref. [11].

The present excitation functions were determined as follows. Since no sharp resonance has been observed in the excitation functions of the photodisintegration of ^{4}He in the energy region up to ~100 MeV, we assumed the excitation functions can be approximated by a fitting function in Ref. [11], i.e.,

$$\sigma(E_\gamma) = \sigma_c \frac{|Q|^a (E_\gamma - |Q|)^b}{E_\gamma^{a+b}}. \quad (1)$$

Three parameters σ_c, a, and b are determined by fitting this functions to the data measured at AIST [36] and the data measured at high energies of $E_\gamma \gtrsim 30$ MeV [41–43] by means of the χ^2-minimization method. This function is suitable for use in numerical calculation because it has no discontinuity and no divergence at high energies. In this study we take published values for errors of cross sections at all fitting procedures.

The most probable fitting functions for the cross sections of the ^{4}He$(\gamma, p)^3$H and ^{4}He$(\gamma, n)^3$He reactions turn out to be

$$\sigma(E_\gamma) = 128.9 \text{ mb} \frac{|Q|^{4.524}(E_\gamma - |Q|)^{2.512}}{E_\gamma^{4.524+2.512}}, \quad (2)$$

and

$$\sigma(E_\gamma) = 31.68 \text{ mb} \frac{|Q|^{3.663}(E_\gamma - |Q|)^{1.580}}{E_\gamma^{3.663+1.580}}, \quad (3)$$

respectively, and they are plotted in Fig. 1. Reaction Q values are taken from experiments as $|Q| = 19.8139$ MeV and $|Q| = 20.5776$ MeV, respectively. We take these two cross sections as our recommended cross sections in this paper.

The dashed-dotted curves are standard expressions from Ref. [11]. Parameter values are given as $\sigma_c = 19.5$ mb, $a = 3.5$, and $b = 1.0$ for ^{4}He$(\gamma, p)^3$H reaction, and $\sigma_c = 17.1$ mb, $a = 3.5$ and $b = 1.0$ for ^{4}He$(\gamma, n)^3$He reaction.

As another implementation, we fit all data adopted in this study including the data measured at AIST [36] at low energies of $E_\gamma < 30$ MeV and previous ones obtained in other experiments. The fitting parameters turn out to be $\sigma_c = 61.82$ mb, $a = 4.300$, and $b = 1.756$ for ^{4}He$(\gamma, p)^3$H reaction, and $\sigma_c = 31.38$ mb, $a = 3.651$, and $b = 1.583$ for ^{4}He$(\gamma, n)^3$He reaction. The derived cross sections are displayed in Fig. 2.

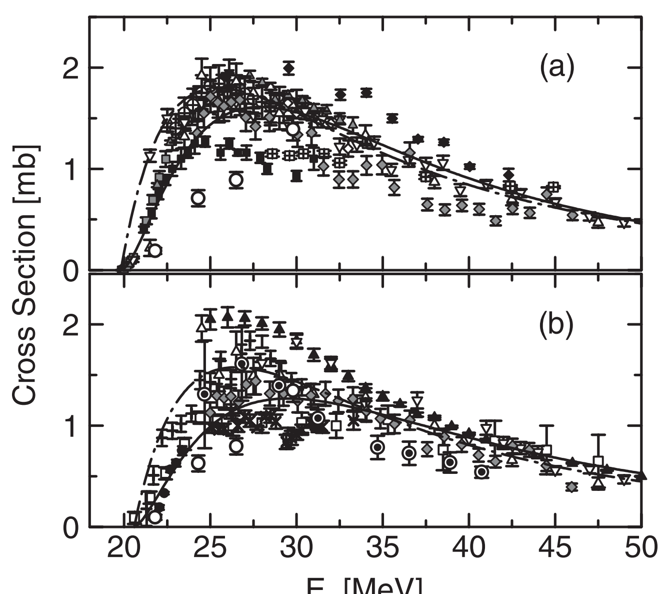

FIG. 2. (a) and (b) are the same as those in Fig. 1. The solid curves and the short-dashed curves are the most probable excitation functions determined from all data adopted in this study, including the experimental data at $E_\gamma \lesssim 30$ MeV [36] and the previous ones at whole energy range of $E_\gamma < 116$ MeV [37,38,41–43,64]. The dashed-dotted curves are the same as in Fig. 1.

One can see in Figs. 1 and 2 that there is a large dispersion in experimental data at low photon energies of 20 MeV $\lesssim E_\gamma \lesssim$ 40 MeV. This dispersion is much larger than the $\pm 1\sigma$ deviation of any single fitting function. We therefore adopt the above three functions in BBN calculations and compare the calculated results with one another in order to study the sensitivity of BBN with the radiative particle decay to the ^{4}He photodisintegration reaction cross sections.

III. BBN OF THE LIGHT ELEMENTS

A. Model

We assume the creation of high-energy photons from the radiative decay of a massive particle X with a mass M_X and a mean life of $\tau_X = 10^2$–10^{12} s. We represent the emitted photon energy by $E_{\gamma 0}$. We assume that the decaying dark particle is nonrelativistic, and almost at rest in the expanding universe.

A decay-produced energetic photon interacts with the cosmic background and induces an electromagnetic cascade shower. The faster processes, pair production through background photons $\gamma_{\rm bg}$ ($\gamma\gamma_{\rm bg} \rightarrow e^+e^-$) and inverse Compton scattering of produced electrons and positrons through background photons ($e^\pm\gamma_{\rm bg} \rightarrow e^\pm\gamma$), produce electromagnetic showers, and the nonthermal photon spectrum realizes a quasistatic equilibrium [44,45]. The attained zeroth-generation photon spectrum is [46]

$$p_\gamma(E_\gamma) \approx \begin{cases} K_0(E_X/E_\gamma)^{1.5} & \text{for } E_\gamma < E_X \\ K_0(E_X/E_\gamma)^{2.0} & \text{for } E_X \leq E_\gamma < E_C, \\ 0 & \text{for } E_C \leq E_\gamma \end{cases} \quad (4)$$

where $K_0 = E_{\gamma 0}/(E_X^2[2 + \ln(E_C/E_X)])$ is a normalization constant fixed by energy conservation of the injected photon energy. This spectrum has a break in the power law at $E_\gamma = E_X$ and an upper cutoff at $E_\gamma = E_C$. We take the same energy scaling with the temperature T of the background photons as in [44], i.e., $E_X = m_e^2/80T$ and $E_C = m_e^2/22T$ at the temperature T, where the cascade spectrum was calculated by numerically solving a set of Boltzmann equations. Here, m_e is the rest mass of an electron.

Because the rates of electromagnetic interactions are faster than the cosmic expansion rate, the photon spectrum $p_\gamma(E_\gamma)$ is modified into a new quasistatic equilibrium (QSE). This distribution is given by

$$\mathcal{N}_\gamma^{\rm QSE}(E_\gamma) = \frac{n_X p_\gamma(E_\gamma)}{\Gamma_\gamma(E_\gamma)\tau_X}, \quad (5)$$

where $n_X = n_X^0(1+z)^3 \exp(-t/\tau_X)$ is the number density of the decaying particles at a redshift z. The quantity Γ_γ is the energy degradation rate through three slower processes; Compton scattering ($\gamma e_{\rm bg}^\pm \rightarrow \gamma e^\pm$), Bethe-Heitler ordinary pair creation in nuclei ($\gamma N_{\rm bg} \rightarrow e^+e^-N$), and double photon scattering ($\gamma\gamma_{\rm bg} \rightarrow \gamma\gamma$) for the zeroth-generation photons. We use this steady state approximation for the cosmic nonthermal constituent of photons.

The equation for the production and destruction of nuclei by nonthermal photons is given by

$$\frac{dY_A}{dt} = \sum_T N_{AC}[T\gamma]_A Y_T - \sum_P [A\gamma]_P Y_A, \quad (6)$$

where we have defined the reaction rate

$$[T\gamma]_A = \frac{n_\gamma^0 \zeta_X}{\tau_X}\left(\frac{1}{2H_r t}\right)^{3/2} \exp(-t/\tau_X) \times \int_0^\infty dE_\gamma S_\gamma^{\rm QSE}(E_\gamma)\sigma_{\gamma+T\rightarrow A}(E_\gamma), \quad (7)$$

and

$$S_\gamma^{\rm QSE}(E_\gamma) = \frac{\tau_X}{E_{\gamma 0} n_X}\mathcal{N}_\gamma^{\rm QSE}(E_\gamma). \quad (8)$$

$Y_i \equiv n_i/n_B$ is the mole fraction of a particular nuclear species i, and n_i and n_B are number densities of nuclei i and baryons. The first and second term on the right-hand side are the source ($\gamma + T \rightarrow A + C$) and sink ($\gamma + A \rightarrow P + D$) terms for nucleus A. E_γ is a nonthermal photon energy. The cross section of the process $\gamma + T \rightarrow A + C$ is denoted by $\sigma_{\gamma+T\rightarrow A}(E_\gamma)$. Further, we use N_{AC} to represent the number of identical species of nuclei in a production or destruction process; $N_{AC} = 2$ when particles A and C are identical and $N_{AC} = 1$ when they are not. For example, in the process ^{4}He(γ, d)D, $N_{\rm DD} = 2$. We defined $H_r \equiv \sqrt{8\pi G\rho_{\rm rad}^0/3}$, where the superscript 0 denotes present values ($z = 0$), therefore n_γ^0 and $\rho_{\rm rad}^0$ are the present photon number density and present radiation energy density of the cosmic background radiation, respectively. We defined $\zeta_X = (n_X^0/n_\gamma^0)E_{\gamma 0}$.

The equation describing the secondary production and destruction is obtained by taking account of the energy loss of nuclear species, while propagating through the background. In general, because of the high energy loss rate, the primary particles establish a quasistatic equilibrium. The abundance evolution is then represented by

$$\frac{dY_S}{dt} = \sum_{T,A,T'} Y_T Y_{T'} \frac{N_{AX_1}N_{SX_2}}{N_{AT'}}[T(A)T']_S - (\text{sink term}), \quad (9)$$

where $[T(A)T']_S$ is the reaction rate for a secondary process $T(\gamma, X_1)A(T', X_2)S$ with any combination of particles X_1, A, and X_2. For example, $[\alpha(^3\mathrm{He})\alpha]_{^6\mathrm{Li}}$ for a secondary process ^{4}He(γ, n)^{3}He(α, p)^{6}Li is given by

$$[\alpha\alpha]_{^6\mathrm{Li}} = \frac{\eta(n_\gamma^0)^2\zeta_X}{\tau_X}\left(\frac{1}{2H_r t}\right)^3 \exp(-t/\tau_X) \times \int_{E_{p,\mathrm{th}}}^{\mathcal{E}_{^3\mathrm{He}}(E_C)} dE_{^3\mathrm{He}} \frac{\sigma_{^3\mathrm{He}(\alpha,p)^6\mathrm{Li}}(E_{^3\mathrm{He}})\beta_{^3\mathrm{He}}}{b_{^3\mathrm{He}}(E_{^3\mathrm{He}})} \times \int_{\mathcal{E}^{-1}_{^3\mathrm{He}}(E_{^3\mathrm{He}})}^{E_C} dE_\gamma S_\gamma^{\mathrm{QSE}}(E_\gamma)\sigma_{^3\mathrm{He}(\alpha,p)^6\mathrm{Li}}(E_\gamma), \quad (10)$$

where η is the baryon-to photon ratio: $\eta \equiv n_B^0/n_\gamma^0$, and β_A is the velocity of the primary particle A. $b_A = -dE/dt$ is the energy loss rate of the primary particle by Coulomb scattering. $\mathcal{E}_A(E_\gamma)$ is the energy of the nuclide A produced by the photodisintegration process $\gamma + T \rightarrow A$, and $\mathcal{E}_A^{-1}(E_A)$ is the energy of the nonthermal photons, which produce the primary species A with energy E_A. $\mathcal{E}_A(E_\gamma)$ and $\mathcal{E}_A^{-1}(E_A)$ are derivable in the limit of low-energy scattering, where the relevant nuclei are nonrelativistic, i.e., $\mathcal{E}_{^3\mathrm{He}}(E_\gamma) = (E_\gamma - E_{\gamma,\mathrm{th}})/4$ and $\mathcal{E}^{-1}_{^3\mathrm{He}}(E_{^3\mathrm{He}}) = 4E_{^3\mathrm{He}} + E_{\gamma,\mathrm{th}}$, where $E_{\gamma,\mathrm{th}}$ is the threshold energy of primary photodisintegration reaction.

B. Constraints on the radiative decay of long-lived particles

We focus on the nonthermal production of mass 3 nuclides, ^{3}H and ^{3}He, and secondary production of ^{6}Li. In Fig. 3, photodisintegration cross sections of ^{4}He$(\gamma, n)^3$He and ^{4}He$(\gamma, p)^3$H are shown as a function of nonthermal photon energy E_γ (above threshold energy 20 MeV). These cross sections are fitted with data from the laser-Compton photon experiment (solid curves) and those from Ref. [11] (dotted curves). The dashed line is the energy spectrum of nonthermal photon produced by the radiative decay when the cosmic temperature is 10 eV corresponding to the decay life $\tau_X \sim 10^{10}$ s [12]. It is normalized with respect to intensity at $E_\gamma = 20$ MeV. Since the yield of nonthermally produced mass 3 nuclides is proportional to the integration of the nonthermal photon spectrum times photodisintegration cross sections, the change of photodisintegration cross sections at $E_\gamma \lesssim 30$ MeV has a relatively large influence on the resulting ^{3}He abundance.

On the other hand, nonthermal secondary production of ^{6}Li is not affected by ^{4}He photodisintegration cross sections at low energies. When we consider the nonrelativistic limit of nuclear reactions, the center-of-mass energy E_{cm} in ^{3}He$(\alpha, p)^6$Li and ^{3}H$(\alpha, n)^6$Li reactions is given by

$$E_{\mathrm{cm}} = \frac{1}{2}\mu v^2 \sim \frac{1}{2}\frac{m_3 m_4}{m_3 + m_4} v_3^2 \sim \frac{4}{7}E_3, \quad (11)$$

where μ, m_3, and m_4 are the reduced mass, the mass of a nucleus ^3A (t or ^{3}He) and that of ^{4}He, v, and v_3 are the relative velocity and the velocity of ^3A, E_3 is the kinetic energy of ^3A, respectively. The energy of ^3A generated in primary ^{4}He$(\gamma, n)^3$He and ^{4}He$(\gamma, p)^3$H reactions, i.e., E_3^0 ($\geq E_3$) is given by

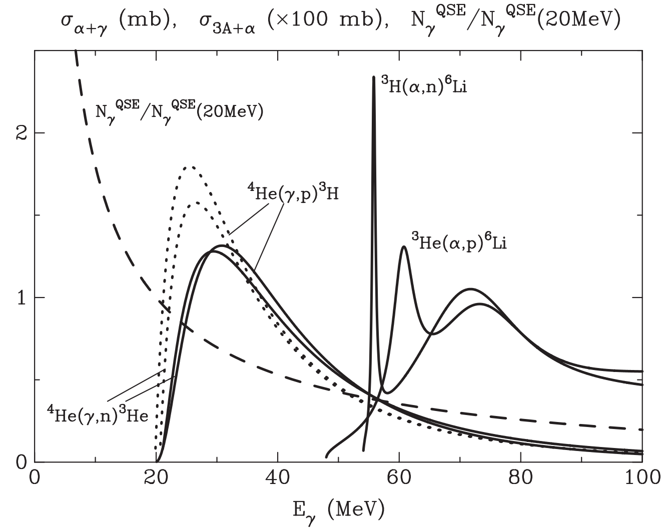

FIG. 3. The fitted cross sections of ^{4}He$(\gamma, n)^3$He and ^{4}He$(\gamma, p)^3$H with data from the laser-Compton photon experiment at low energies of $E_\gamma \lesssim 30$ MeV are shown by solid lines above $\sim$20 MeV. The standard cross sections [11] are also shown as dotted lines. Cross sections of secondary ^{6}Li production reactions ^{3}H$(\alpha, n)^6$Li and ^{3}He$(\alpha, p)^6$Li are superimposed. The energy spectrum of nonthermal photon produced by the radiative decay when the cosmic temperature is 10 eV corresponding to the decay life $\tau_X \sim 10^{10}$ s is also shown (dashed line), which is normalized with respect to intensity at $E_\gamma = 20$ MeV.

$$E_3^0 \sim \frac{m_p}{m_3 + m_p}(E_\gamma - E_{\gamma,\mathrm{th}}) \sim \frac{1}{4}(E_\gamma - E_{\gamma,\mathrm{th}}), \quad (12)$$

where m_p is the mass of proton, and $E_{\gamma,\mathrm{th}}$ is the threshold energy of the ^{4}He photodisintegration reaction. The center-of-mass energy E_{cm} in the secondary reactions thus relates to the nonthermal photon energy in primary reactions as

$$E_{\mathrm{cm}} \lesssim \frac{E_\gamma - E_{\gamma,\mathrm{th}}}{7}. \quad (13)$$

The inequality means that nonthermal ^{3}He and ^{3}H nuclides lose energies from a time of their production to a time of nuclear reactions to produce ^{6}Li. We plot the cross sections of ^{3}He$(\alpha, p)^6$Li and ^{3}H$(\alpha, n)^6$Li reactions as a function of E_γ neglecting the energy losses of ^{3}He and ^{3}H in Fig. 3. Since secondary ^{6}Li production needs photon energy of at least $E_\gamma \gtrsim 50$ MeV to produce energetic ^{3}He and ^{3}H, the yield of ^{6}Li is insensitive to the change of the ^{4}He photodisintegration cross section at the low energy of $E_\gamma \lesssim 30$ MeV. (See Sec. III B 1.) On the other hand, a change of the cross section at high energies of $E_\gamma \gtrsim 50$ MeV causes a change of resulting yield of ^{6}Li (See Sec. III B 2 for estimation of uncertainty on the ^{6}Li yield associated with possible uncertainties in cross sections at high energies.)

1. Effect of uncertainties from low-energy reactions

Figure 4 shows contours corresponding to the constraints for the primordial abundance [12] for the present result with our recommended smaller cross sections of ^{4}He photodisintegration Eqs. (2) and (3) [thick lines]. For example, a contour of the ^{4}He mass fraction $Y > 0.232$ is shown in the (τ_X, ζ_X) plane. The region above this contour should be excluded for $Y < 0.232$. The contours of ^{7}Li/H lower limit, $^7\text{Li/H} > 1.1 \times 10^{-10}$, D/H upper and lower limits, $\text{D/H} \leq 5.2 \times 10^{-5}$ and $\text{D/H} \geq 1.4 \times 10^{-5}$ (dashed line), respectively, and ^{3}He/H upper limit, $^3\text{He/H} \leq 3.1 \times 10^{-5}$ are also drawn. Dotted lines show contours of the same constraints for the result with larger standard cross sections of ^{4}He photodisintegration [11]. The thick solid line shows a constraint from the consistency requirement of the CMB with a blackbody [12]. The region above the line is excluded. The contour for the MPHSs level of $^6\text{Li/H} = 6.6 \times 10^{-12}$ is plotted. The gray region above the contour and below the nucleosynthesis plus CMB constraints is allowed and abundant in ^{6}Li.

For this figure, we use the two sigma upper limit on the observed ^{3}He/H abundance ratio from the Galactic HII region [47] as a conservative constraint on primordial abundance. Alternatively, a constraint from the ^{3}He/D ratio is often used. Since deuterium is fragile and more easily burned in stars than ^{3}He is, the ^{3}He/D ratio is thought to increase monotonically as a function of time by stellar processing from the formation of first stars to the solar system formation. The ^{3}He/D ratio for primordial abundances can, therefore, be constrained by the solar ^{3}He/D ratio. Since the solar ^{3}He/D ratio is $(^3\text{He/D})_\odot = 0.82$ [48], one can obtain a constraint of $^3\text{He/D} < 1$ for primordial abundances. Although this constraint is slightly stronger than the constraint for the ^{3}He/H ratio, the contours for both constraints are not distinguishable from each other in Fig. 4.

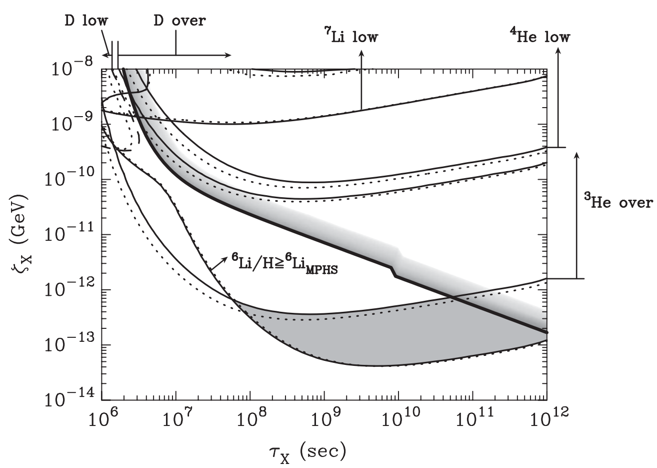

FIG. 4. Contours in the (τ_X, ζ_X) plane corresponding to the adopted constraints for the primordial abundances in the present calculation with smaller cross sections of ^{4}He photodisintegration Eqs. (2) and (3) [thick lines]. Contours for the mass fraction of ^{4}He $Y = 0.232$ and the number ratios of $^3\text{He/H} = 3.1 \times 10^{-5}$, $\text{D/H} = 5.2 \times 10^{-5}$, $\text{D/H} = 1.4 \times 10^{-5}$ (dashed line), and $^7\text{Li/H} = 1.1 \times 10^{-10}$ are shown. The notation "over" and "low" identifies overproduced and underproduced regions, respectively. The same constraints on the result calculated with larger standard cross sections of ^{4}He photodisintegration [11] is shown as dotted lines. The region above the thick solid line is excluded by the consistency requirement of the CMB with a blackbody. The contour of $^6\text{Li/H} = 6.6 \times 10^{-12}$ is also drawn. The gray region above the contour and below the nucleosynthesis plus CMB constraints is the allowed region where the abundant ^{6}Li is produced.

One can see that ^{7}Li abundance does not change drastically by the new ^{4}He photodisintegration cross sections. The contour for the ^{4}He over destruction by the nonthermal photons shifts upward by $\sim$300% at most for $\tau_X = 10^6$–10^{10} s with respect to that with the larger cross sections (dotted line). Since a destruction rate of ^{4}He is lowered at low energies when its cross sections are taken to be small, larger energy is necessary to destruct ^{4}He considerably. The ^{4}He destruction leads to nonthermal production of ^{3}He and D. Then, D over-destruction regions, which are above the region of this figure, shift upward reflecting the change of relic abundance of seed nuclide ^{4}He. The ^{3}He over-production region also shifts upward by $\sim$30%. Since the cross sections of $^4\text{He}(\gamma, p)^3\text{H}$ and $^4\text{He}(\gamma, n)^3\text{He}$ are lowered, the amount of produced mass 3 nuclides is lowered. One finds an upward shift of D over-production region. We confirmed that this change is caused since D is produced by $p(n, \gamma)\text{D}$ using nonthermally produced neutrons by $^4\text{He}(\gamma, n)^3\text{He}$, whose cross section changed. Figure 4 shows that the contour of ^{6}Li abundance also changes slightly by $\sim -20\%$ at most for

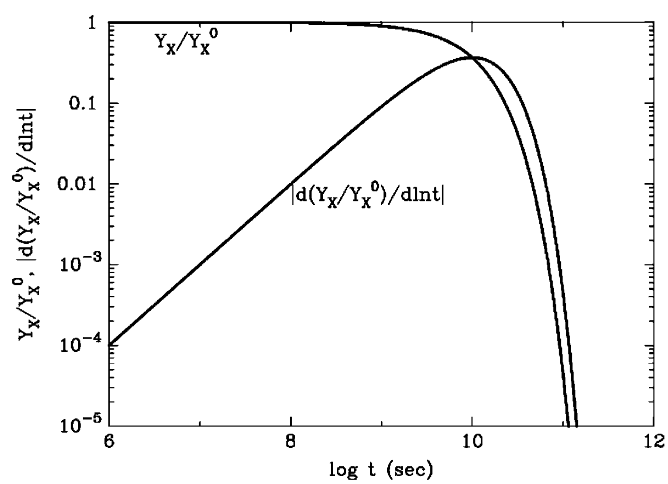

FIG. 5. Time evolution of abundance of X particles Y_X/Y_X^0, where Y_X^0 is the initial abundance before X decays. Also shown is $t \times |d(Y_X/Y_X^0)/dt| = (t/\tau_X)\exp(-t/\tau_X)$, which characterizes the amount of energy from the particle decay at time t. The decay life is assumed to be $\tau_X = 10^{10}$ s.

$\tau_X = 10^6$–10^{10} s, but this change does not result from the change of photodisintegration cross sections of ^{4}He at low energy $E_\gamma \lesssim 30$ MeV. It is due to the difference of excitation functions between our recommended fit and the standard fit [11] at higher energy, $E_\gamma \gtrsim 30$ MeV. (See Fig. 3.) The reason has already been explained at the beginning of this section.

We pick up the most interesting parameter region, where ^{6}Li is produced at the level higher than that of MPHSs. We take a look at the result of nucleosynthesis of the parameters $(\tau_X, \zeta_X) = (10^{10}$ s, 3×10^{-13} GeV) [12] for this reason. In Fig. 5, the abundance of X particle Y_X is shown as a function of the cosmic photon temperature. It is normalized as Y_X/Y_X^0, where Y_X^0 is the initial abundance before the X decay decreases its abundance. As the indicator of energy amount injected by the X decay at an epoch, we also plot $|d(Y_X/Y_X^0)/d\ln t| = t \times |d(Y_X/Y_X^0)/dt| = (t/\tau_X) \times \exp(-t/\tau_X)$. Most of the energy content is injected in the time scale of τ_X. These lines are for only the case of $\tau_X = 10^{10}$ s.

Figure 6 shows the ^{3}He and ^{3}H abundances as a function of temperature T [$T_9 \equiv T/(10^9$ K)] when parameters are $(\tau_X, \zeta_X) = (10^{10}$ s, 3×10^{-13} GeV) [upper panel]. The results with our recommended and the standard cross sections of ^{4}He photodisintegration correspond to the solid and dashed lines, respectively. An apparent reduction of nonthermally produced ^{3}He abundance is found in our recommended case. The resulting difference of nonthermal yield of ^{3}He is about 10%.

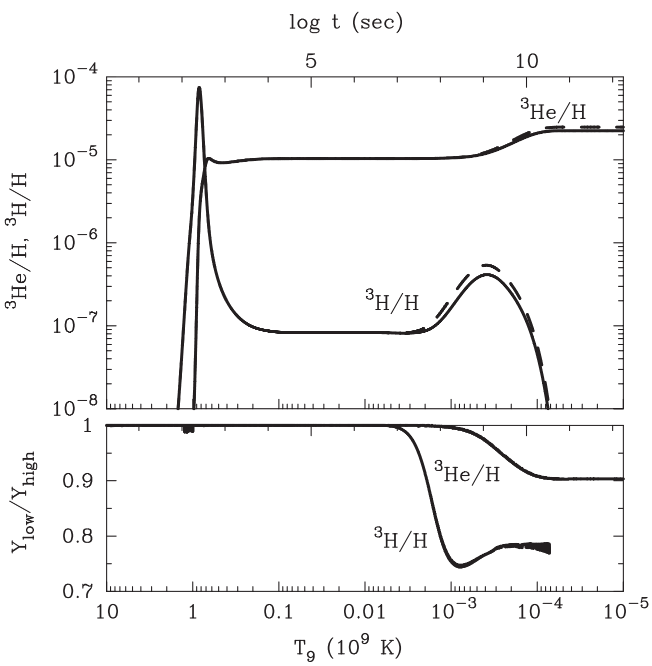

FIG. 6. (upper panel) Temperature (time) evolution of ^{3}He and ^{3}H abundances when parameters are $(\tau_X, \zeta_X) = (10^{10}$ s, 3×10^{-13} GeV). The solid and dashed lines are the results for our recommended and the standard cross sections of ^{4}He photodisintegration. (lower panel) Ratios of ^{3}He and ^{3}H abundances calculated with our recommended cross sections to those with the standard cross sections.

2. *Effect of uncertainties from high-energy reactions*

The measured ^{4}He photodisintegration cross sections are still subject to large uncertainties, which depend on the different experimental setup and methods over the wide energy range. The energy dependence of the cross sections is not well understood theoretically. If either cross section of ^{4}He$(\gamma, p)^3$H or ^{4}He$(\gamma, n)^3$He in the energy region of $E_\gamma \gtrsim 50$ MeV is different from the adopted cross section, nonthermal BBN abundance of ^{6}Li would change significantly.

It should be noted here that the data below 30 MeV of Shima *et al.* [36] are significantly smaller than previous ones, and therefore one may expect enhancement of the cross sections in the higher energy range from the well-known Thomas-Reiche-Kuhn (TRK) sum rule, which relates the energy-integrated cross section σ_0 to the ground state property of a target nucleus. The E1 sum rule is expressed by

$$\sigma_0 = \int_{E_{\rm th}}^{\infty} \sigma(E_\gamma) dE_\gamma = \sigma_{\rm TRK}(1+\kappa) = 59.74(1+\kappa) \text{ MeV mb}, \tag{14}$$

where $\sigma_{\rm TRK} = (2\pi^2\alpha/m)(NZ/A)$ with α, m, N, Z, and A the fine structure constant, the nucleon mass, the neutron number, the proton number, and the nucleon number, respectively. κ is the so-called TRK enhancement factor defined as

$$\kappa = \frac{mA}{NZ}\langle 0|[D_z, [V, D_z]]|0\rangle, \tag{15}$$

where $|0\rangle$ is the nuclear ground state wave function, D_z is the dipole operator $D_z = \sum_{i=1}^{A} z_i \tau_i^3/2$ with τ_i^3 and z_i the third component of the isospin operator and the z coordinate of the ith particle in the center-of-mass frame, respectively, V is the nuclear potential. There is another sum rule, i.e., bremsstrahlung sum rule, which is expressed by

$$\sigma_B = \int_{E_{\rm th}}^{\infty} \frac{\sigma(E_\gamma)}{E_\gamma} dE_\gamma = 4\pi^2\alpha\langle 0|D_z D_z|0\rangle = \frac{4\pi^2\alpha}{3}\frac{NZ}{A-1}(\langle r_\alpha^2\rangle - \langle r_p^2\rangle) = 2.60 \pm 0.01 \text{ mb}, \tag{16}$$

where $\langle r_p^2\rangle^{1/2} = 0.875 \pm 0.007$ fm [49] and $\langle r_\alpha^2\rangle^{1/2} = 1.673 \pm 0.001$ fm [50] are the root mean square charge radii for proton and ^{4}He, respectively.

Energy-weighted integrals $\int_{E_{\rm th}}^{\infty} (E_\gamma)^n \sigma(E_\gamma) dE_\gamma$ with $n = 0$ for Eq. (14) and $n = -1$ for Eq. (16) are listed in Table I for the four different models of photodisintegration cross sections of ^{4}He$(\gamma, p)^3$H and ^{4}He$(\gamma, n)^3$He. The three

TABLE I. Energy-weighted integrals of photodisintegration cross sections $\sigma(E_\gamma)$ in Eqs. (14) and (16).

Models for $\sigma(E_\gamma)$	Equations (2) and (3)	Fit with all data[a]	Cyburt *et al.* [11][b]	Sum rule[c]
σ_0 [MeV mb]	77.7	79.7	84.4	118.[d]
σ_B [mb]	1.94	2.08	2.32	2.60

[a]Equation (1) with $|Q| = 19.8139$ MeV, $\sigma_c = 61.82$ mb, $a = 4.300$, and $b = 1.756$ for ^{4}He$(\gamma, p)^3$H, and $|Q| = 20.5776$ MeV, $\sigma_c = 31.38$ mb, $a = 3.651$, and $b = 1.583$ for ^{4}He$(\gamma, n)^3$He.
[b]Equation (1) with $|Q| = 19.8139$ MeV, $\sigma_c = 19.5$ mb, $a = 3.5$, and $b = 1.0$ for ^{4}He$(\gamma, p)^3$H, and $|Q| = 20.5776$ MeV, $\sigma_c = 17.1$ mb, $a = 3.5$, and $b = 1.0$ for ^{4}He$(\gamma, n)^3$He.
[c]The functions derived by fitting Eq. (1) to the data obtained at AIST [36] in $E_\gamma \lesssim 29.8$ MeV are modified at higher energies so that the energy-weighted integrals satisfy two sum rules; Eq. (1) with $\sigma_c = 21.0$ mb, $a = 1.68$, and $b = 1.88$ for ^{4}He$(\gamma, p)^3$H, and $\sigma_c = 16.8$ mb, $a = 1.41$, and $b = 1.73$ for ^{4}He$(\gamma, n)^3$He (for $E_\gamma \leq 29.8$ MeV) and $\sigma(E_\gamma) = 2.65$ mb$(E_\gamma/29.8\ \mathrm{MeV})^{-5/2}$ (for $E_\gamma > 29.8$ MeV).
[d]Value derived from $\sigma_0 = 59.7(1 + \kappa)$ with $\kappa \approx 1$ [51–54].

models of our recommended fit, i.e., Eqs. (2) and (3), the fit with all data adopted in this study, and the standard fit [11] lead to values smaller than the sum rules, i.e., $\sigma_0 = 59.7(1 + \kappa)$ MeV mb with $\kappa \approx 1$ for the TRK sum rule and $\sigma_B = 2.60 \pm 0.01$ mb for the bremsstrahlung sum rule. We expect that the model using Eqs. (2) and (3) is closer to the lower limit of true cross sections in consideration of two sum rules.

In addition to the three models in the second, third, and fourth columns in Table I mentioned above, we make another new fitting function of the cross sections so that the energy-weighted integrals satisfy the two sum rules: As for low-energy cross sections at $E_\gamma \lesssim 30$ MeV, we fit the experimental data [36] measured by using quasimonochromatic laser-Compton photon beams at AIST. At higher energy $E_\gamma \gtrsim 30$ MeV, we assume a simple energy dependence $\sigma(E_\gamma) = \sigma_C(E_\gamma/29.8\ \mathrm{MeV})^{-N/2}$. Resultant parameters are $\sigma_c = 2.65$ mb and $N = 5$. In this new model where we require the sum rules, the constructed cross sections are typically $\gtrsim 2$ times larger than our recommended ones at 50 MeV $\lesssim E_\gamma \lesssim$ 135 MeV, where the upper limit is the meson mass. Both the TRK sum rule and bremsstrahlung sum rule do not apply to such high energies $E_\gamma \gtrsim 135$ MeV because new degrees of freedom of mesons as well as nucleons play an important role, and the above two sum rules break down. We can expect that the constructed cross sections, which satisfy the sum rules are, close to the upper limits to the realistic cross sections.

We compare the primordial abundance calculated with new cross sections, which satisfy the sum rules and that of our recommended cross sections. In Fig. 7 thick solid and dashed lines correspond to the results with our recommended and new cross sections of ^{4}He photodisintegration, respectively. The dark and light gray regions above the solid and dashed contour lines and below the nucleosynthesis plus CMB constraints are the allowed region, where the abundant ^{6}Li is produced. The ^{6}Li production occurs more efficiently in the case with larger cross sections than with smaller ones. This is because the ^{4}He destruction is more effective for larger cross sections at higher energies so that the more abundant energetic mass 3 nuclides that synthesize ^{6}Li are produced. For this reason the ^{6}Li abundance produced by using the large ^{4}He-photodisintegration cross sections, which satisfy the sum rules, are presumed to be a maximum yield from the viewpoint of nuclear structure physics. The allowed region of the properties of relic X particle in the (τ_X, ζ_X) plane, therefore, should not move even below the light gray region in Fig. 7, and we expect that the reality is located between the dark and light gray regions.

However, it has been known that σ_0 highly depends on various effects of residual interactions among nucleons such as the meson-exchange currents [55], the tensor correlations [51,52], the short-range interactions [53], and so on. In the case of ^{4}He, the calculated values of σ_0, which were integrated out up to $E_\gamma \sim 135$ MeV, have uncertainty

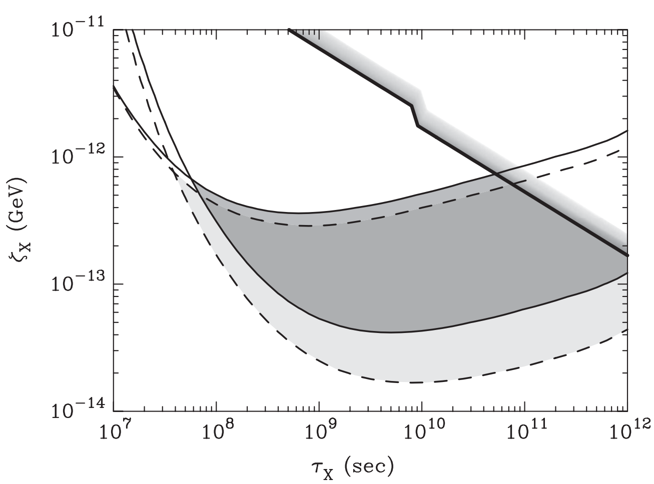

FIG. 7. Contours in the (τ_X, ζ_X) plane corresponding to the adopted constraints for the primordial abundances in the calculation with our recommended cross sections of ^{4}He photodisintegration (thick lines) and those satisfying sum rules (dashed lines). The adopted abundance constraints on light elements are the same as those in Fig. 4. The dark (for our recommended cross sections) and light (for larger ones) gray regions above the solid and dashed contour lines, respectively, and below the nucleosynthesis plus CMB constraints are the allowed region where abundant ^{6}Li is produced.

of more than $\pm 10\%$, depending on the nucleon-nucleon potentials and the nuclear models for the ground state of ^{4}He [53,54,56,57]. In summary, both the existing experimental data and the theoretical calculations for the ^{4}He photodisintegration cross section in the energy range up to $\sim$135 MeV contain large uncertainties, and therefore a precise measurement of the ^{4}He photodisintegration cross section at $E_\gamma \gtrsim 30$ MeV is highly desirable. Comprehensive theoretical study of the nuclear structure and reactions of ^{4}He are also necessary in order to clarify many unresolved nuclear effects and also refine the applicability of an empirical formula such as Eq. (1). These nuclear physics studies would be important to constrain the lifetime and the abundance of long-lived relic X particle more precisely.

IV. SUMMARY AND OUTLOOK

A recent measurement of ^{4}He photodisintegration reactions, $^4\mathrm{He}(\gamma, p)^3\mathrm{H}$ and $^4\mathrm{He}(\gamma, n)^3\mathrm{He}$ with laser-Compton photons shows lower cross sections at low energies than those estimated by other previous experiments. We studied the sensitivity of nonthermal BBN of all light elements D, T, ^{3}He, ^{4}He, ^{6}Li, ^{7}Li, and ^{7}Be to the photodisintegration cross section of ^{4}He.

The change of cross sections of ^{4}He photodisintegration has an influence on the nonthermal yields of light elements, D, ^{3}He, and ^{4}He, which are related to the photodisintegration cross sections at low energy (~ 30 MeV). The upper limit of allowed regions of the X-abundance parameter ζ_X for these light nuclei shifts upward by $\sim 300 - 30\%$ for $\tau_X = 10^6$–10^{10} s for this change of the cross sections. This arises from the upshift of ^{3}He abundance contour (See Fig. 4). On the other hand, the nonthermal ^{6}Li production is not very sensitive to the change of cross sections at low energy, since the nonthermal secondary synthesis of ^{6}Li needs energetic photons of $E_\gamma \gtrsim 50$ MeV.

The nonthermal nucleosynthesis triggered by the radiative particle decay is one of candidates of the production mechanism of ^{6}Li observed in MPHSs. In the interesting parameter region of $10^8\ \mathrm{s} \lesssim \tau_X \lesssim 10^{12}\ \mathrm{s}$ and $5 \times 10^{-14}\ \mathrm{GeV} \lesssim \zeta_X \lesssim 5 \times 10^{-13}\ \mathrm{GeV}$, which satisfies the ^{6}Li production above the abundance level observed in MPHSs, the lowering of the photodisintegration cross sections at low energy $E_\gamma \lesssim 30$ MeV as measured in the recent experiment using laser-Compton photons leads to $\sim$10% reduction of resulting ^{3}He abundance, whereas the ^{6}Li abundance does not change for the change of the cross sections of $^4\mathrm{He}(\gamma, p)^3\mathrm{H}$ and $^4\mathrm{He}(\gamma, n)^3\mathrm{He}$.

Let us briefly discuss other impacts of such a precise cross section measurement. Clarifying the effects of photodisintegrations of ^{4}He will affect more strongly the ν process in core-collapse supernova (SN) explosions through the neutrino-nucleus interactions specifically of $\nu + {}^4$He. The weak transition rates for $^4\mathrm{He}(\nu, \nu')$, $^4\mathrm{He}(\nu_e, e^-)$, and $^4\mathrm{He}(\bar{\nu}_e, e^+)$ are determined similarly to the giant electric dipole resonance observed in the photodisintegrations with the help of theoretical calculation [58]. In fact, several experiments of measuring the ^{4}He photodisintegration cross sections [36] were carried out for this purpose. The precise knowledge of the $^4\mathrm{He}(\nu, \nu' p)$, $(\nu, \nu' n)$, $(\nu_e, e^- p)$, and $(\bar{\nu}_e, e^+ n)$ cross sections is required to determine the unknown parameters for neutrino oscillations through the Mikheyev-Smirnov-Wolfenstein effect on the ^{7}Li and ^{11}B production triggered by the $\nu + {}^4$He reactions [59,60]. The energy range $E_\nu = 10$–25 MeV is very important for the ν-process nucleosynthesis in SNe. The mean neutrino energy of SN neutrinos is presumed to be about 10–25 MeV in numerical simulations of the neutrino transfer in core-collapse SNe, and the threshold energies for all neutrino-induced spallation reactions of ^{4}He are $\sim$20 MeV. Therefore, the difference between the newly measured [36] and previous ^{4}He photodisintegration cross sections at $20\ \mathrm{MeV} \lesssim E_\gamma \lesssim 30$ MeV could be critical. As a result, the absolute yields of ^{7}Li and ^{11}B produced in the ν process in core-collapse SNe would be different from one another, depending on the assumed ν-process reaction rates as demonstrated theoretically [58,61], although the ratio of $^7\mathrm{Li}/^{11}\mathrm{B}$ does not change largely.

Another recent focus of photodisintegration of ^{4}He is on the mechanism of the core-collapse SNe. Most SN simulations still do not succeed in the SN explosion in spite of detailed numerical studies of the neutrino transfer calculations inside the core. Haxton [62] proposed that the neutrino-induced excitations of ^{4}He and heavier nuclei could deposit extra energy to the ejected materials and revive the shockwave, which motivated a recent theoretical study on the role of ^{4}He spallation reactions in the core-collapse SNe [63]. His theoretical suggestion also motivated recent experimental studies of photodisintegrations of ^{4}He [36] in order to estimate the neutrino-induced reaction cross sections for $^4\mathrm{He}(\nu, \nu')$, $^4\mathrm{He}(\nu_e, e^-)$, and $^4\mathrm{He}(\bar{\nu}_e, e^+)$.

As such, it is important and even critical to study the $^4\mathrm{He}(\gamma, p)$ and $^4\mathrm{He}(\gamma, n)$ reactions precisely for the discussions of the problem of SN-neutrino oscillation and SN explosion as well as the cosmological discussion concerning the BBN with a radiative decay of long-lived relic particles.

ACKNOWLEDGMENTS

This work has been supported in part by the Mitsubishi Foundation, the Grant-in-Aid for Scientific Research under Contract Nos. 17540275 and 20244035 of the Ministry of Education, Science, Sports and Culture of Japan, and the JSPS Core-to-Core Program, International Research Network for Exotic Femto Systems (EFES). M. K. acknowledges the support by JSPS Grant-in-Aid under Contract No. 18.11384.

[1] D. N. Spergel *et al.* (WMAP Collaboration), Astrophys. J. Suppl. Ser. **148**, 175 (2003).
[2] D. N. Spergel *et al.* (WMAP Collaboration), Astrophys. J. Suppl. Ser. **170**, 377 (2007).
[3] S. G. Ryan, T. C. Beers, K. A. Olive, B. D. Fields, and J. E. Norris, Astrophys. J. **530**, L57 (2000).
[4] J. Melendez and I. Ramirez, Astrophys. J. **615**, L33 (2004).
[5] M. Asplund, D. L. Lambert, P. E. Nissen, F. Primas, and V. V. Smith, Astrophys. J. **644**, 229 (2006).
[6] S. Inoue, W. Aoki, T. K. Suzuki, S. Kawanomoto, A. E. García-Pérez, S. G. Ryan, and M. Chiba, IAU Symposium / Symp-Int.Astron.Union **228**, 59 (2005).
[7] R. Cayrel *et al.*, Astron. Astrophys. **473**, L37 (2007).
[8] K. Jedamzik, Phys. Rev. D **74**, 103509 (2006).
[9] K. Jedamzik, Phys. Rev. Lett. **84**, 3248 (2000).
[10] M. Kawasaki, K. Kohri, and T. Moroi, Phys. Rev. D **63**, 103502 (2001).
[11] R. H. Cyburt, J. Ellis, B. D. Fields, and K. A. Olive, Phys. Rev. D **67**, 103521 (2003).
[12] M. Kusakabe, T. Kajino, and G. J. Mathews, Phys. Rev. D **74**, 023526 (2006).
[13] K. Jedamzik, Phys. Rev. D **70**, 063524 (2004).
[14] K. Jedamzik, Phys. Rev. D **70**, 083510 (2004).
[15] M. Kawasaki, K. Kohri, and T. Moroi, Phys. Rev. D **71**, 083502 (2005).
[16] D. Cumberbatch, K. Ichikawa, M. Kawasaki, K. Kohri, J. Silk, and G. D. Starkman, Phys. Rev. D **76**, 123005 (2007).
[17] In a parameter region of $\tau_X \sim 3 \times 10^6$ s and $\zeta_X \sim 10^{-9}$ GeV, ^{6}Li and ^{7}Li problems seem to be fixed [11,12,18], where the ^{7}Li abundance decreases because of ^{7}Be destruction by a primary ^{7}Be(γ, ^{3}He)^{4}He reaction. It is, however, found that in this parameter region where ^{7}Li abundance decreases by photodissociation to the level of the ^{7}Li plateau, either the D abundance was too low or the number ratio ^{3}He/D was too large. This is absolutely excluded in light of standard stellar evolution and chemical evolution [18].
[18] J. R. Ellis, K. A. Olive, and E. Vangioni, Phys. Lett. B **619**, 30 (2005).
[19] O. Richard, G. Michaud, and J. Richer, Astrophys. J. **619**, 538 (2005).
[20] D. L. Lambert, AIP Conf. Proc. **743**, 206 (2004).
[21] M. Pospelov, Phys. Rev. Lett. **98**, 231301 (2007).
[22] K. Hamaguchi *et al.*, Phys. Lett. B **650**, 268 (2007).
[23] R. H. Cyburt *et al.*, J. Cosmol. Astropart. Phys. 11 (2006) 014.
[24] K. Kohri and F. Takayama, Phys. Rev. D **76**, 063507 (2007).
[25] C. Bird, K. Koopmans, and M. Pospelov, Phys. Rev. D **78**, 083010 (2008).
[26] M. Kusakabe, T. Kajino, R. N. Boyd, T. Yoshida, and G. J. Mathews, Phys. Rev. D **76**, 121302(R) (2007).
[27] M. Kusakabe, T. Kajino, R. N. Boyd, T. Yoshida, and G. J. Mathews, Astrophys. J. **680**, 846 (2008).
[28] M. Kawasaki, K. Kohri, and T. Moroi, Phys. Lett. B **649**, 436 (2007).
[29] M. Kawasaki, K. Kohri, T. Moroi, and A. Yotsuyanagi, Phys. Rev. D **78**, 065011 (2008).
[30] T. Jittoh, K. Kohri, M. Koike, J. Sato, T. Shimomura, and M. Yamanaka, Phys. Rev. D **76**, 125023 (2007).
[31] T. Jittoh, K. Kohri, M. Koike, J. Sato, T. Shimomura, and M. Yamanaka, Phys. Rev. D **78**, 055007 (2008).
[32] K. Jedamzik, Phys. Rev. D **77**, 063524 (2008).
[33] K. Jedamzik, J. Cosmol. Astropart. Phys. 03 (2008) 008.
[34] M. Pospelov, arXiv:0712.0647.
[35] M. Pospelov, J. Pradler, and F. D. Steffen, J. Cosmol. Astropart. Phys. 11 (2008) 020.
[36] T. Shima *et al.*, Phys. Rev. C **72**, 044004 (2005).
[37] S. Nakayama *et al.*, Phys. Rev. C **76**, 021305(R) (2007).
[38] T. Yamagata *et al.*, Phys. Rev. C **74**, 014309 (2006).
[39] T. Kii, T. Shima, T. Baba, and Y. Nagai, Nucl. Instrum. Methods Phys. Res., Sect. A **552**, 329 (2005).
[40] T. Shima *et al.* (unpublished).
[41] A. N. Gorbunov, Phys. Lett. **27B**, 436 (1968).
[42] Yu. M. Arkatov *et al.*, Sov. J. Nucl. Phys. **19**, 598 (1974).
[43] C. K. Malcom, D. V. Webb, Y. M. Shin, and D. M. Skopik, Phys. Lett. **47B**, 433 (1973).
[44] M. Kawasaki and T. Moroi, Astrophys. J. **452**, 506 (1995).
[45] R. J. Protheroe, T. Stanev, and V. S. Berezinsky, Phys. Rev. D **51**, 4134 (1995).
[46] V. S. Berezinskii, S. V. Bulanov, V. A. Dogiel, V. L. Ginzburg, and V. S. Ptuskin, *Astrophysics of Cosmic Rays*, edited by V. S. Verezinskii and V. L. Ginzburg (North-Holland, New York, 1990).
[47] T. M. Bania, R. T. Rood, and D. S. Balser, Nature (London) **415**, 54 (2002).
[48] K. Lodders, Astrophys. J. **591**, 1220 (2003).
[49] W. M. Yao *et al.* (Particle Data Group), J. Phys. G **33**, 1 (2006).
[50] E. Borie and G. A. Rinker, Phys. Rev. A **18**, 324 (1978).
[51] K. Okamoto and K. Hasegawa, Prog. Theor. Phys. **28**, 137 (1962).
[52] A. Arima, G. E. Brown, H. Hyuga, and M. Ichimura, Nucl. Phys. **A205**, 27 (1973).
[53] D. Gazit, N. Barnea, S. Bacca, W. Leidemann, and G. Orlandini, Phys. Rev. C **74**, 061001(R) (2006).
[54] W. T. Weng, T. T. S. Kuo, and G. E. Brown, Phys. Lett. **46B**, 329 (1973).
[55] M. Gari and H. Hebach, Phys. Lett. **49B**, 29 (1974).
[56] M. Fink, M. Gari, and H. Hebach, Phys. Lett. **49B**, 20 (1974).
[57] I. Elminyawi and J. S. Levinger, Phys. Rev. C **28**, 82 (1983).
[58] T. Suzuki, S. Chiba, T. Yoshida, T. Kajino, and T. Otsuka, Phys. Rev. C **74**, 034307 (2006).
[59] T. Yoshida, T. Kajino, H. Yokomakura, K. Kimura, A. Takamura, and D. H. Hartmann, Phys. Rev. Lett. **96**, 091101 (2006).
[60] T. Yoshida, T. Kajino, H. Yokomakura, K. Kimura, A. Takamura, and D. H. Hartmann, Astrophys. J. **649**, 319 (2006).
[61] T. Yoshida *et al.*, Astrophys. J. 686, 448 (2008).
[62] W. C. Haxton, Phys. Rev. Lett. **60**, 1999 (1988).
[63] N. Ohnishi, K. Kotake, and S. Yamada, Astrophys. J. **641**, 1018 (2006).
[64] B. Nilsson *et al.*, Phys. Rev. C **75**, 014007 (2007).